Hindawi
Shock and Vibration
Volume 2020, Article ID 5845712, 10 pages
https://doi.org/10.1155/2020/5845712

Research Article

Mitigating Large Vibrations of Stayed Cables in Wind and Rain Hazards

Hung Vo-Duy[1] and Cung H. Nguyen[2]

[1]*The University of Da Nang-University of Science and Technology, Da Nang, Vietnam*
[2]*Department of Civil Engineering, Industrial University of Ho Chi Minh City, Ho Chi Minh City 700 000, Vietnam*

Correspondence should be addressed to Cung H. Nguyen; nguyenhuycung@iuh.edu.vn

Received 20 February 2020; Accepted 1 May 2020; Published 19 May 2020

Academic Editor: Vasant Matsagar

This paper presents an experimental investigation of stayed cable vibrations in dry-wind and rain-wind coupling hazards. To mitigate large vibrations of the cable, the use of spiral wires wrapped around the cable is proposed. By testing two cable models in a wind tunnel in dry and rain conditions for different yaw angles and wind speeds, the effectiveness of using the spiral wires to mitigate large vibrations is clarified. Finally, the paper provides a further understanding of the complex mechanism of wind-induced and rain-wind-induced vibrations. It is found that the low-frequency vortex flows in the wake play a significant role in the excitation of large responses of the cable in high wind speeds. The spiral wires dismiss these low-frequency flows and then reduce the large vibrations.

1. Introduction

Stay cables, such as members of cable-stayed bridges, are very sensitive to wind loading, leading to large oscillation amplitudes, even to collapses due to aeroelastic instability. They are also vulnerable to large vibrations due to rain-wind coupling actions. Study on aerodynamics and aeroelasticity of cables has attracted much interest for many years. It has been shown that common types of large vibrations of cables include vortex-induced vibration (VIV), galloping, and rain-wind-induced vibrations (RWIV). The studies on these topics have not only focused on understanding the physics and mechanics of the phenomena but also provided methods to mitigate the vibrations.

It is well known that the classical VIV occurs when a Von Karman vortex is shed with a frequency close to structural frequency. This resonance then results in large vibrations. For an inclined cable, an axial vortex flow exits along the cable and near the wake. It interacts and mitigates Von Karman vortex and then excites large vibrations of the cable in high wind speeds. The role of the axial vortex on large vibrations of cables and its mechanism has been investigated though pioneering studies by Matsumoto and his colleagues [1–6]. The phenomenon related to these large amplitude vibrations of cables in dry condition was referred to as dry galloping and also considered as a special case of VIV due to the presence of the axial vortex. It has been recognised that wind flow around inclined cables as well as aerodynamic and aeroelastic behaviour of the cables is sophisticated that needs further investigations.

In the 21st century, a number of studies on dry galloping of inclined cables have been conducted in different parts of the world. In an attempt to explain the mechanism of dry galloping of inclined cables, Macdonald [7] used quasisteady theory to predict successfully the occurrence of galloping that was observed in wind tunnel tests by Cheng et al. [8]. Macdonald's study shows that drag crisis in the critical Reynolds number range causes the dry galloping. Later, quasisteady conditions for the occurrence of galloping of inclined cables were developed [9, 10]. Wind tunnel experiments on cables have been carried out to understand further the phenomenon [11–17]. Despite many efforts, the mechanism of excitation of large vibrations of cables remains unclear and therefore is deserved for further investigations.

The first report on violent vibrations of stay cables in the coupling of rain and wind actions was provided by Hikami and Shiraishi [18] based on full-scale measurement. The field observations on this phenomenon were documented later by other researchers [19–23]. Due to the nature of complexity and uncertainty in field measurement, it is difficult to clarify the mechanism of RWIV. A number of wind tunnel experiments on cable models have been conducted to understand the phenomenon. To simulate rain water on cables, fixed artificial water rivulets were attached on the cable surface [2, 24], or liquids were sprayed on the cables [25–29]. Recently, rain simulators were employed in wind tunnel to have better rainfall simulations, in which rainfall intensity can be adjusted in the tests [30, 31]. According to those studies, the existence of axial flows, water rivulets, and thin waters plays significant roles in RWIV. However, their roles as individuals or as combinations have not been clearly understood [31].

In order to mitigate large responses of stayed cables in dry and rain conditions, two main approaches have been applied in research as well as in real practices. The first method is to use one or two external damper devices attached near a cable anchorage, such as viscous dampers, fluid dampers, tuned mass dampers, tuned inerter dampers, and magnetorheological dampers. Although there are many studies on dynamic properties and effectiveness of those dampers for the mitigation of structural vibrations [32–36], very few studies are on how these dampers affect the occurrence of large vibrations of cables in winds. Nguyen and Macdonald [37] first addressed the galloping issue of a taut cable with an attached viscous damper.

In the second method, cables are wrapped with single or multiple spiral protuberance wires (helical fillets). The efficiency of this method has been shown through wind tunnel tests. For example, a series of experiments in the wind tunnel of Yokohama National University successfully used the spiral wires to reduce dry galloping [38, 39]. Larose and Smitt [27] reported an effective application of a single spiral protuberance for mitigating RWIV. Nevertheless, full-scale monitoring at Øresund Bridge reported that the use of spiral wires was not effective as initially expected [23].

The above remarks have motivated this study, in which vibrations of two cable models in dry and rain conditions were studied by means of wind tunnel tests. One of the models is a circular cylinder with smooth surface. Another is as the same as the smooth cylinder but is wrapped with spiral wires as a proposed method for mitigating large responses of the cable in dry-wind and rain-wind coupling. Rainfall was simulated through a rain simulator system, which allows controlling the rain intensity and provides better and more realistic rain modelling compared with others in the literature. Finally, mechanism of the large vibrations of the two models was investigated that provides a further understanding of the complex phenomena of wind flows which passed an inclined cable.

The paper is structured into five main sections. Section 2 presents the details of the wind tunnel testing setup and results of the measurement of the aeroelastic responses of the two cable models in dry and rain conditions. Section 3 explains the mechanism of the large vibrations of the circular cable through the measurement of the flow field in the wake of the fixed cable. Section 4 presents the further tests on the fixed cable wrapped by spiral wires to assess the reduction of the large vibrations of the cable. Finally, critical comments are provided in Section 5.

2. Vibrations of Cables in Dry Wind and Rain Wind and Their Mitigations

2.1. Setup of Wind Tunnel Tests. Wind tunnel tests on two stay cable models were conducted in a wind tunnel of the Yokohama National University. The wind tunnel has a working section with the dimension of 1.3 m width and 1.8 m height. The maximum wind speed is about 20 m/s.

Model 1 is a plain high-density polyethylene (HDPE) tube of 158 mm diameter and 1500 mm length (Figure 1(a)). Model 2 is the same as Model 1 but is wrapped with 12 spiral protuberances (Figure 1(b)). The spiral wires were arranged with a spiral angle of 27°. The dimensions of each spiral wire are 7.5 mm width and 5 mm height.

The cable models were supported by a system of springs allowing the vibrations only in vertical direction, i.e., normal to the wind flow, as one-degree-of-freedom (1DOF) system. The orientation of the cable with respect to the wind flow is determined through the angles α, β, and γ defined as in Figure 2. The angles a and β are commonly referred to as inclination angle and yaw angle, respectively. The tests were conducted for an inclination angle $\alpha = 25^\circ$ and four yaw angles $\beta = 0^\circ$, 15°, 30°, and 45° in smooth wind with dry and rain conditions.

Rain was simulated by a system of water nozzles located up-front of the Model (front wind) and at the ceiling of the working section of the wind tunnel (Figure 3). The rainwater was sprayed from these nozzles to the cable models. The rain volume can be controlled through a volume adjustment system located outside the wind tunnel.

In the arrangement of measurement systems, dynamic pressure and wind speed were measured by a Pitot Tube. An accelerator system was used to capture cable vibrations in time. Each accelerometer has a rate capacity of 49.03 m/s^2. To measure the cable vibrations, an accelerometer was mounted at each end of the cable. The vibrations were recorded for a duration of 60 seconds with the sampling frequency 50 Hz.

The structural, wind, and rain parameters used in the tests are given in Table 1. For each yaw angle β, dynamic parameters of the cable models, including the fundamental frequency f_s (Hz) and damping ratio ξ (%), were estimated from free vibration tests and showed in Table 2.

2.2. Wind-Induced Responses of the Circular Cable in Dry and Rain Conditions. Figures 4(a) and 4(b) show the reduced amplitudes, y_r, of the cable displacements versus reduced wind velocity, U_r, in dry and rain conditions, respectively, for different yaw angles. The reduced amplitude and reduced wind speed are defined as follows:

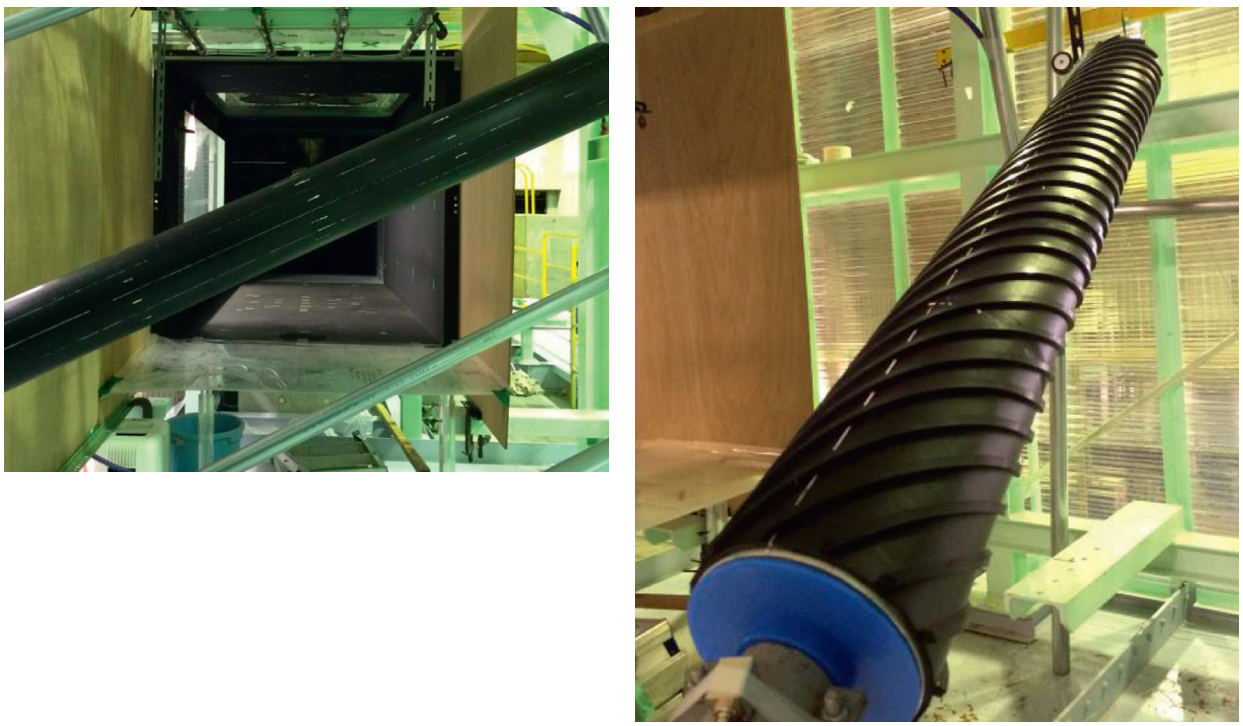

(a) (b)

Figure 1: Spiral protuberance cable Model.

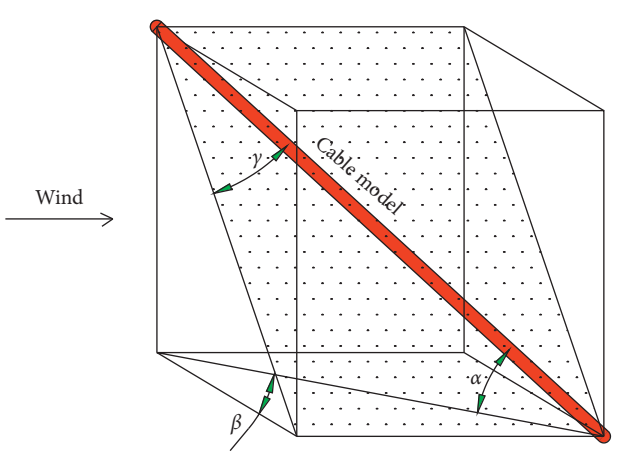

Figure 2: Definition of cable angles.

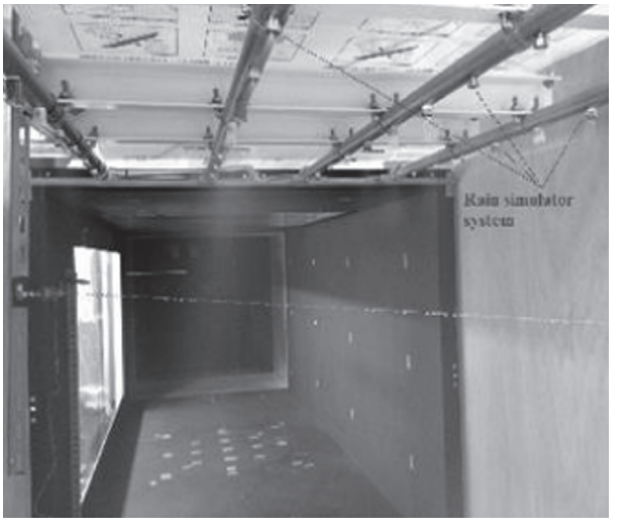

Figure 3: Rain simulator system.

$$y_r = \frac{y}{D}, \qquad U_r = \frac{U}{f_s D}, \tag{1}$$

where y, U, and f_s are the maximum amplitude (peak-to-peak displacement response, unit: m), inlet wind velocity (m/s), and structural fundamental frequency (Hz), respectively.

For dry condition, it can be seen from Figure 4(a) that the responses are generally larger for higher wind speeds. Among the four yaw angles β, the cable exposes to smallest responses for $\beta = 0^\circ$ (when wind is normal to the cable plane)

Table 1: Structural, wind, and rain parameters.

Parameters	Value
Rain volume (mm/h)	40–50
Cable diameter: D (mm)	158
Effective length: L (mm)	1500
Inclination angle: α (°)	25
Mass: m (kg/m)	9.9 (Model 1) 10.8 (Model 2)
Reynolds number	$0–2.1 \times 10^5$

Table 2: Dynamic parameters of cable Models for different yaw angles.

	$\beta = 0^\circ$		$\beta = 15^\circ$		$\beta = 30^\circ$		$\beta = 45^\circ$	
	f_s	ξ	f_s	ξ	f_s	ξ	f_s	ξ
Model 1 (circular)	0.9	0.16	0.9	0.14	0.86	0.16	0.86	0.16
Model 2 (spiral)	0.88	0.14	0.86	0.11	0.86	0.16	0.86	0.14

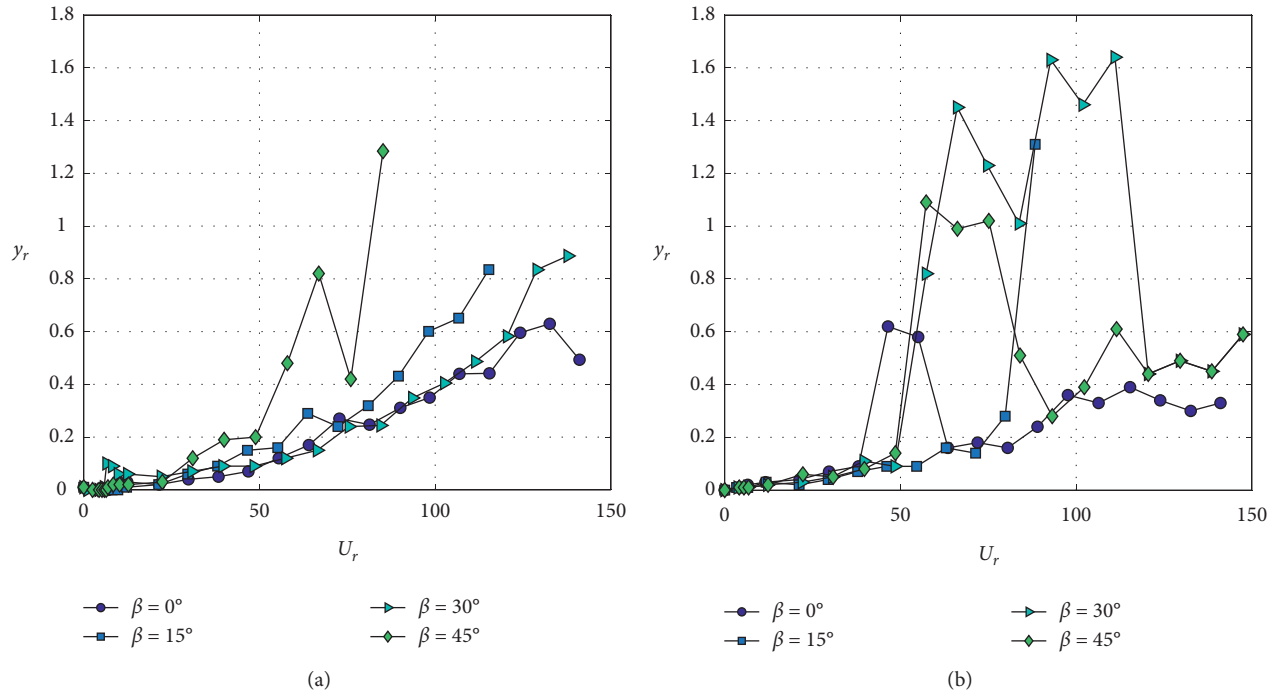

Figure 4: Wind-induced responses of circular cable in dry condition (a) and rain condition (b).

and largest responses for $\beta = 45^\circ$. For most of the cases, the amplitudes increase for increasing reduced wind speed. For $\beta = 45^\circ$, there is a sudden reduction of amplitude at $U_r = 76$. The reduction of amplitude is also seen for $\beta = 0^\circ$ and $\beta = 15^\circ$ but less significant. This amplitude reduction feature has been previously observed in the literature [5, 12, 17, 30]. In addition to Figure 4(a), at a given reduced wind speed, the cable does not vibrate with larger amplitudes for higher β as seen that the responses for $\beta = 15^\circ$ are larger than those for $\beta = 30^\circ$. For a range of low reduced wind speeds from 0 to 15, there is an apparent peak response for $\beta = 30^\circ$ at $U_r = 6.5$, looking similar to the classical vortex-induced vibration (VIV) due to Von Karman vortex. For other yaw angles, observation of VIV responses is not clear. This will be explained in the next section.

For rain condition, the vibration amplitudes do not always increase for increasing wind speeds. Instead, for each yaw angle, the amplitude is increasing for increased wind speed but significantly reduced at a higher wind speed as seen in Figure 4(b). These shapes of the responses are typical for rain-wind-induced vibration (RWIV) of cables as documented widely in the literature [3, 18, 24].

Comparing the responses of the cable in rain and dry condition, it reveals that, depending on the value of the reduced wind speed, the cable in wind condition can expose larger or smaller vibration amplitudes. Taking $\beta = 30^\circ$ as an example, for $U_r = 57.3$–111, the cable vibrates violently in rain condition with amplitudes much larger, up to 4 times, than those without rain. However, for stronger wind with reduced speed higher than 111, rain can lead to reduction of cable vibrations. In summary, rain can be beneficial for the cable vibrating in high wind but significantly detrimental for the cable in a certain rain of wind speeds.

2.3. Mitigating Cable Vibrations with Spiral Wires. Section 2.2 has shown the large vibration amplitudes of the smooth cylinder (Model (1) in both cases with and without rain. To mitigate the large responses, 12 spiral wires were used to wrap around the smooth cable. The experimental results on the spiral cable (Model (2)) are shown below.

Figure 5 plots the reduced amplitudes of the cable with (w) and without (w/o) using spiral wires in rain and dry conditions for various yaw angles. The substantial reductions of vibration amplitudes can be seen when the cable is wrapped with the wires. This shows the efficiency of using spiral wires as a method to mitigate the cable vibrations.

Looking at the vibrations of the cable with the spiral wires, their amplitudes generally increase for increasing wind speeds, both in rain and without rain. Also, it can be

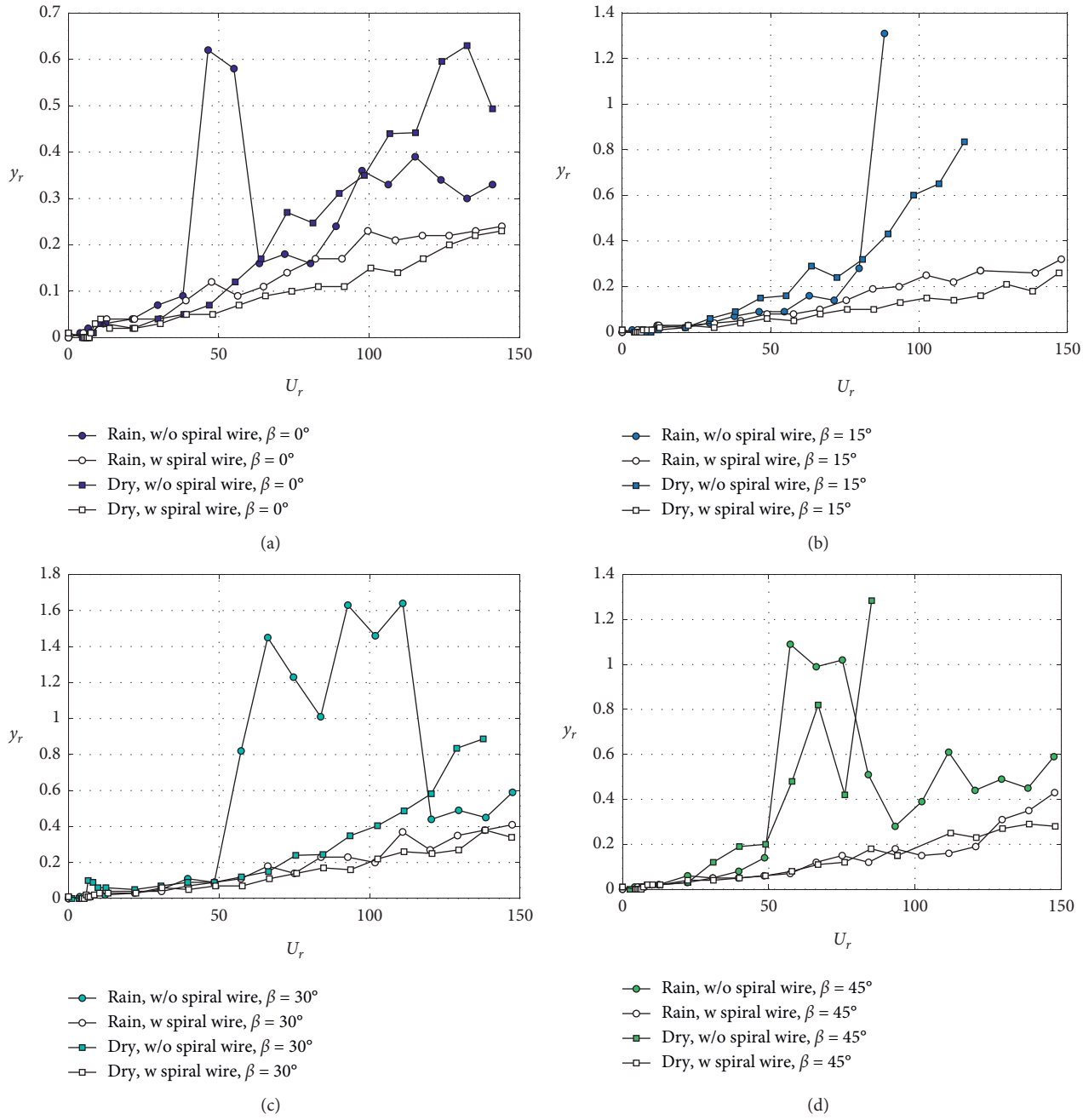

FIGURE 5: Reduced amplitudes of cable vibrations with and without using spiral wire in rain and dry condition for (a) $\beta = 0^\circ$, (b) $\beta = 15^\circ$, (c) $\beta = 30^\circ$, and (d) $\beta = 45^\circ$.

observed from Figures 5(a)–5(c) that, for yaw angles $\beta = 0^\circ$, $\beta = 15^\circ$, and $\beta = 30^\circ$, wind induces larger vibration amplitudes in rain than in dry condition. For $\beta = 45^\circ$, the vibration amplitudes in rain are larger or smaller than in dry condition, depending on the wind speed.

In addition to the vibrations of the cable with the spiral wires, particularly in rain, the variation of the amplitudes of Model 2 (with the spiral wires) against wind speeds has different pattern from those of Model 1 (without the spiral wires). The later has been discussed in the previous section in relation to Figure 4. As shown in many studies [28, 31, 40], the formation and vibration of water rivulets on the cable in rain give rise to large amplitude vibrations of cables without spiral wires. The appearance of the spiral wires herein interrupts the oscillations of water rivulets on the cable, reducing cable vibrations and changing their patterns.

3. Mechanism of Large Amplitude Vibrations of the Circular Cable

Since the cable exposes to large amplitude vibrations as shown in Figure 4, it is important to understand the mechanism of cable vibrations in wind. For this purpose,

vertical component of fluctuating velocity in the wake of the cable is investigated through further wind tunnel tests.

In the experimental setup, the circular cable (Model 1) was statically fixed in the wind tunnel for $\alpha = 25^\circ$ and $\beta = 30^\circ$. A hot-wire anemometer was used to measure the fluctuating wind speed in the wake of the cable. As illustrated in Figure 6, it is located in the wake of the cable with the coordinates of 0.5D and 2D and varied along the cable with distances from 2D to 7D, allowing the fluctuating speeds to be measured at different locations.

Due to technical difficulty in measuring the fluctuations using hot-wire anemometer in rain, only dry condition was considered during the measurements. For the interest of understanding the flow in the wake of cable in rain, readers might refer to the studies mentioned in Section 1, which used artificial rivulets.

Figure 7 shows the power spectral density (PSD) of the vertical fluctuating wind velocity in the wake along the cable at different locations X, which is a distance from the top end of the cable to the measured location, for $\alpha = 25^\circ$ and $\beta = 30^\circ$. The inlet mean wind velocities in the wind tunnel are 5 m/s (Figure 7(a)), 10 m/s (Figure 7(b)), and 15 m/s (Figure 7(c)). The reduced frequency, denoted as f_r as in the figure, is defined as

$$f_r = \frac{f_w D}{U}, \tag{2}$$

where f_w is the frequency of the vertical fluctuating velocity.

For the inlet wind speed $U = 5$ m/s, as shown in Figure 7(a), there are slight PSD peaks at reduced frequency $f_r = 0.15$; that is, Strouhal number St = 0.15. Such St implies the Von Karman vortex of the circular cable [3, 5, 14], leading to the classical VIV, theoretically at a critical wind speed $U_r = 1/\mathrm{St} = 6.67$. This explains the peak amplitude at $U_r = 6.5$ in the dynamic tests as shown in Figure 4(a), showing the excellent agreement between the theoretical prediction and experiment.

The situation changes for the inlet wind speed 10 m/s. It can be seen from Figure 7(b) that the dominant PSD peaks are at a low reduced frequency $f_r = 0.013$, equivalent to a relatively high reduced velocity $U_r = 76.9$. The appearance of this low-frequency flow weakens the Von Karman vortex as seen in Figure 7(b) and generates larger responses for higher wind speed than those for $U_r = 6.5$ (Figure 4(a)).

It can be seen from Figure 7(c) that when the inlet wind speed increases to 15 m/s, Von Karman vortex is significantly mitigated and two clear PSD peaks appear at reduced frequencies $f_{r1} = 0.009$ and $f_{r2} = 0.017$, equivalent to reduced velocities $U_{r1} = 111$ and $U_{r2} = 58.8$, respectively. To have a further insight into these peaks, Figure 8 shows the wavelet map of the fluctuating wind velocity at the location $X = 6$D, which is near the middle of the cable. The Morlet wavelet mother function was used in the wavelet transform. It can be observed that the mode associated with the reduced frequency f_{r1} is dominant between the two modes and more consistent in time. From (2), the flow at this mode has a frequency of 0.85 Hz, which is close to the structural frequency; therefore, it excites large vibrations of the cable at the high reduced wind speed U_{r1}.

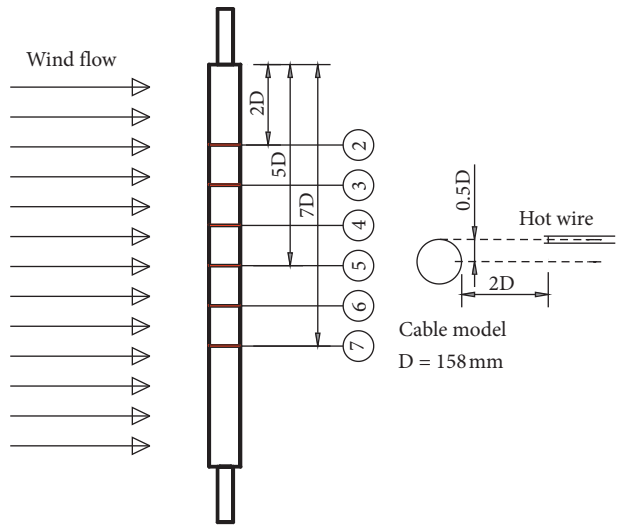

Figure 6: Locations of the hot-wire anemometer in the wake and along the cable.

In summary of the observations from Figures 7 and 8, it is evident that the low-frequency flows in the wake of the cable are more dominant and Von Karman vortex is weaker for higher wind speed. These low-frequency flows contain high energy at high wind speed and so excite large vibrations of the cable. The phenomenon was referred to as dry galloping, according to important investigations by Matsumoto and his colleagues with similar observations [2, 5]. These studies showed that low-frequency axial flows along the cable and near the wake are the main cause of large responses at high wind speeds. On the other hand, in the present study, the low-frequency flows are associated with vertical fluctuation. This implies three-dimensional characteristics of the low-frequency flows in the wake of the cable. This remark agrees CFD simulations of wind flow which passed a yawed cable in [41].

To have a further illustration of the dominating vortices as increasing wind speed and to summarise the mechanism of the large vibrations, Figure 9 shows the normalised PSD, denoted as S_n and given by (3), against the reduced frequency for different wind speeds:

$$S_n = \frac{\mathrm{PSD}}{\sigma_v}, \tag{3}$$

where σ_v is the standard deviation of the vertical fluctuating wind speed in the wake.

It can be seen from Figure 9 that Von Karman vortex is apparent at low reduced wind speed. When the wind speed is increasing, this vortex is gradually suppressing. At the same time, low-frequency flows are developing and getting stronger for higher wind speeds. The low-frequency flows contain high energy that excites the vibration of the cable to higher amplitudes for higher wind speeds.

4. Mechanism of Vibration Stabilisation of the Cable with Spiral Wires

For further understanding how spiral wires can help reducing large vibrations of the cable, it is important to

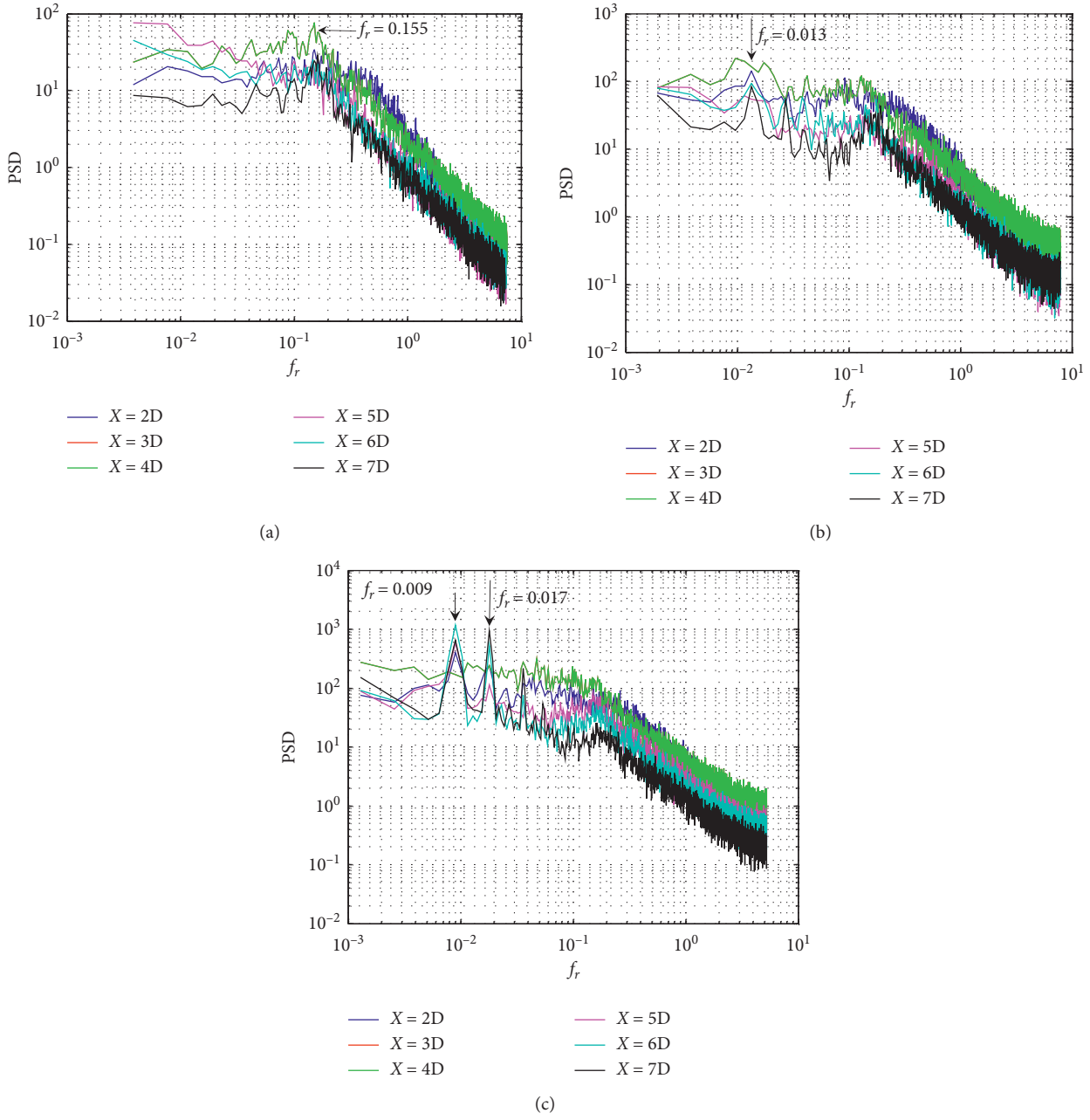

Figure 7: PSD of vertical fluctuating wind speeds for different locations in the wake of the cable, (a) $U = 5$ m/s; (b) $U = 10$ m/s; (c) $U = 15$ m/s.

investigate the vibration mechanism of the cable when it is wrapped with the spiral wires. For this purpose, the vertical component of the fluctuating wind speeds in the wake of Model 2 (Figure 1(b)) was measured. The experimental setup for this measurement with the use of hot wire was the same as described in Section 3, with the same inclination angle and yaw angle; that is, $\alpha = 25^\circ$ and $\beta = 30^\circ$. The inlet wind flow is smooth with the speed $U = 15$ m/s.

Figure 10 compares the spectrums of the vertical fluctuating wind speeds at the location $X = 6$D, i.e., near the middle of the cable, for Model 1 (without spiral wires) and Model 2 (with spiral wires). It can be seen that the dominant spectrum in the low-frequency regime is significantly mitigated when the cable is wrapped with the spiral wires. As these low-frequency vortices are weaken, their energies are too low to excite large vibrations in high wind speeds.

With the presence of the spiral protuberance, the dominant spectrum associates with Von Karman vortex (St = 0.2). Then, the critical reduced velocity for the occurrence of Von Karman VIV is 1/St = 5. For higher wind speeds, the vortex's frequency is different from the frequency of the cable. As a result, the VIV is diminished, showing small amplitude vibrations of the cable.

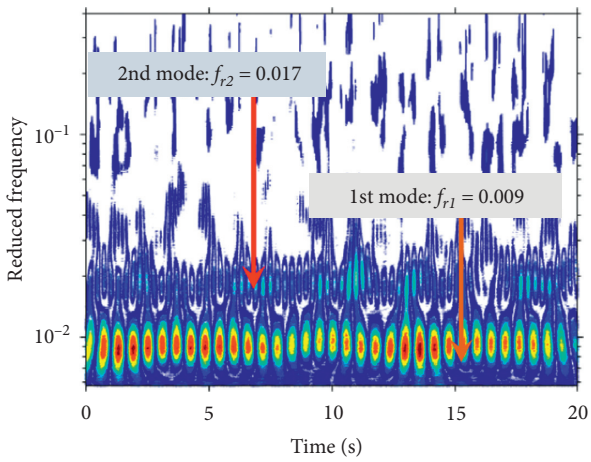

Figure 8: Wavelet map of the vertical fluctuatinag wind speed in the wake at location $X = 6D$ for $\alpha = 25^{\circ}$, $\beta = 30^{\circ}$, and $U = 15$ m/s.

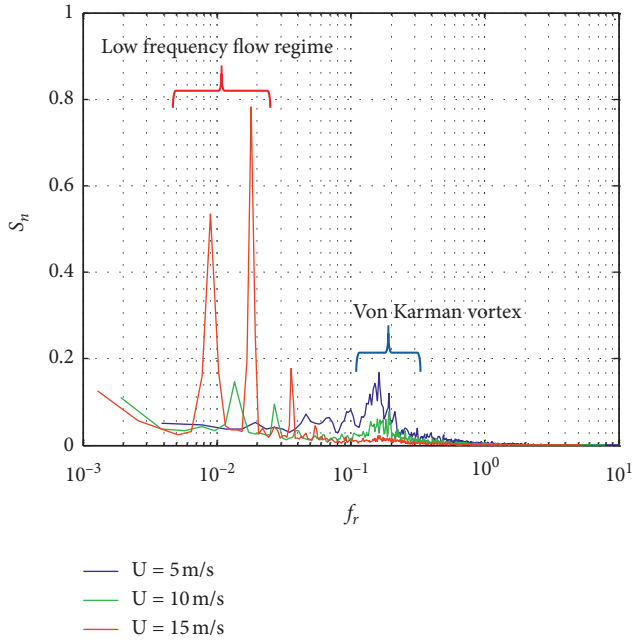

Figure 9: Normalized PSD (location 6D, $D = 158$ mm, $\beta = 30^{\circ}$, and $\alpha = 25^{\circ}$).

5. Conclusions

This paper studies the vibration characteristics of stayed cables in wind with and without rain through a series of wind tunnel experiments. A rain simulator system in which rain intensity can be controlled was used to simulate a more realistic rainfall and water on the cable surface. The tests were conducted for four yaw angles (0°, 15°, 30°, and 45°). Also, the use of spiral protuberance wires wrapping around the cable as a method to mitigate cable vibrations is investigated.

The tests on the smooth cable (without spiral wires) showed that, in dry condition, Von Karman VIV was apparent for yaw angle 30° and weak for other yaw angles. Meanwhile in rain condition, VIV disappeared for all

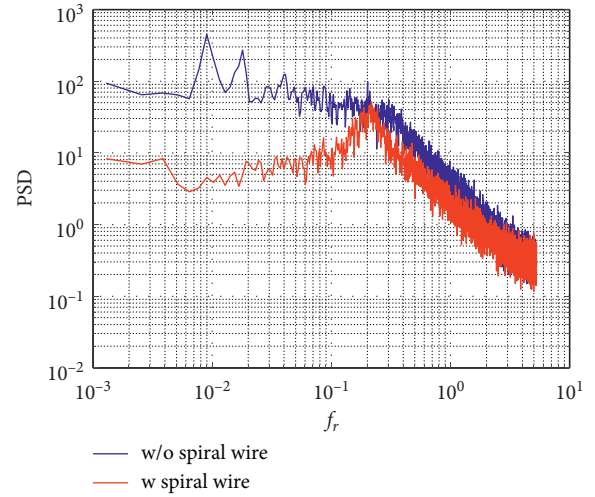

Figure 10: PSD of fluctuating wind speed in the wake of Model 1 (cable without the spiral wires) and Model 2 (with the spiral wires).

angles. In addition, for each yaw angle, RWIV with large amplitudes were observed for a range of wind speeds. These amplitudes were larger, up to 4 times, than those without rain. For higher wind speeds outside this range, the amplitudes were significantly reduced. Among tested yaw angles, for the both cases with and without rain, the cable is exposed to smaller vibration amplitudes when being normal to the wind (zero yaw angle) than when being yawed to the wind.

On the other hand, the tests on the cable wrapped with the spiral wires showed considerable reduction of vibrations amplitudes in both dry and rain conditions. Typical RWIV were then suppressed, although they had slightly larger amplitudes than in dry condition. This observation implies the role of the spiral wires in mitigating the larger responses of cable in wind hazards with and without the coupling of rain.

In an attempt to understand the mechanism of the large amplitude vibrations as well as the mechanism of mitigating such amplitudes, the vertical fluctuations in the wake of the cable models were measured. The low-frequency vortex flows were found. They play a vital role in generating large responses of the smooth cable in high wind speeds. These vortices interrupt the Von Karman vortex, shed continuously and regularly in time, and contain high energy that excites the vibration of the cable. When the spiral wires were wrapped around the cable, they dismissed the low-frequency flows and so reduced the vibration amplitudes.

Data Availability

Data used to support the findings of this study are available from the corresponding author upon request.

Conflicts of Interest

The authors declare that there are no conflicts of interest regarding the publication of this paper.

Acknowledgments

This research was funded by Vietnam National Foundation for Science and Technology Development (NAFOSTED) under Grant no. 107.04–2017.321. The authors gratefully acknowledge the support from the Department of Civil Engineering, Yokohama National University, for the wind tunnel experiments.

References

[1] M. Matsumoto, "Aerodynamic behaviour of inclined circular cylinders-cable aerodynamics," *Wind Engineering and Industrial Aerodynamics*, vol. 33, pp. 63–72, 1990.

[2] M. Matsumoto, N. Shiraishi, and H. Shirato, "Rain-wind induced vibration of cables of cable-stayed bridges," *Journal of Wind Engineering and Industrial Aerodynamics*, vol. 43, no. 1-3, pp. 2011–2022, 1992.

[3] M. Matsumoto, T. Yagi, Y. Shigemura, and D. Tsushima, "Vortex-induced cable vibration of cable-stayed bridges at high reduced wind velocity," *Journal of Wind Engineering and Industrial Aerodynamics*, vol. 89, no. 7-8, pp. 633–647, 2001.

[4] M. Matsumoto, T. Yagi, Q. Liu, Y. Oishi, and Y. Adachi, "Effects of axial flow and Karman vortex interference on dry-state galloping of inclined stay-cables," in *Proceedings of the 6th International Symposium on Cable Dynamics*, pp. 247–254, Charleston, SC, USA, September 2005.

[5] M. Matsumoto, T. Yagi, H. Hatsuda, T. Shima, M. Tanaka, and H. Naito, "Dry galloping characteristics and its mechanism of inclined/yawed cables," *Journal of Wind Engineering and Industrial Aerodynamics*, vol. 98, no. 6-7, pp. 317–327, 2010.

[6] T. Tanaka, M. Matsumoto, H. Ishizaki, and H. Kibe, "Dry galloping characteristic and vibration control of inclined stay cable," in *Proceedings of the First International Symposium on Flutter and its Application*, pp. 639–648, Tokyo, Japan, 2016.

[7] J. H. G. Macdonald, "Quasi-steady analysis of 2DOF inclined cable galloping in the critical Reynolds number range," in *Proceedings of the 6th International Symposium on Cable Dynamics*, pp. 435–442, Charleston, SC, USA, September 2005.

[8] S. Cheng, P. A. Irwin, J. B. Jakobsen, and G. L. Larose, "Divergent motion of cables exposed to skewed wind," in *Proceedings of the 5th International Symposium on Cable Dynamics*, pp. 271–278, Charleston, SC, USA, September 2003.

[9] J. H. G. Macdonald and G. L. Larose, "A unified approach to aerodynamic damping and drag/lift instabilities, and its application to dry inclined cable galloping," *Journal of Fluids and Structures*, vol. 22, no. 2, pp. 229–252, 2006.

[10] J. H. G. Macdonald and G. L. Larose, "Two-degree-of-freedom inclined cable galloping-Part 1: general formulation and solution for perfectly tuned system," *Journal of Wind Engineering and Industrial Aerodynamics*, vol. 96, no. 3, pp. 291–307, 2008.

[11] H. Katsuchi and H. Yamada, "Dry galloping characteristics of indented stay cables in turbulent flow," in *Proceedings of the 9th International Symposium on Cable Dynamics*, Shanghai, China, October 2011.

[12] J. B. Jakobsen, T. L. Andersen, J. H. G. Macdonald et al., "Wind-induced response and excitation characteristics of an inclined cable Model in the critical Reynolds number range," *Journal of Wind Engineering and Industrial Aerodynamics*, vol. 110, pp. 100–112, 2012.

[13] N. Nikitas and J. H. G. Macdonald, "Aerodynamic forcing characteristics of dry cable galloping at critical Reynolds numbers," *European Journal of Mechanics-B/Fluids*, vol. 49, pp. 243–249, 2015.

[14] W. Ma, Q. Liu, J. H. G. Macdonald, X. Yan, and Y. Zheng, "The effect of surface roughness on aerodynamic forces and vibrations for a circular cylinder in the critical Reynolds number range," *Journal of Wind Engineering and Industrial Aerodynamics*, vol. 187, pp. 61–72, 2019.

[15] N. Nikitas, J. H. G. MacDonald, J. B. Jakobsen, and T. L. Andersen, "Critical Reynolds number and galloping instabilities: experiments on circular cylinders," *Experiments in Fluids*, vol. 52, no. 5, pp. 1295–1306, 2012.

[16] W. Ma, J. H. G. Macdonald, Q. Liu, C. H. Nguyen, and X. Liu, "Galloping of an elliptical cylinder at the critical Reynolds number and its quasi-steady prediction," *Journal of Wind Engineering and Industrial Aerodynamics*, vol. 168, 2017.

[17] G. Matteoni and C. T. Georgakis, "Effects of surface roughness and cross-sectional distortion on the wind-induced response of bridge cables in dry conditions," *Journal of Wind Engineering and Industrial Aerodynamics*, vol. 136, pp. 89–100, 2015.

[18] Y. Hikami and N. Shiraishi, "Rain-wind induced vibrations of cables stayed bridges," *Journal of Wind Engineering and Industrial Aerodynamics*, vol. 29, no. 1-3, pp. 409–418, 1988.

[19] M. Matsumoto, "Observed behavior of prototype cable vibration and its generation mechanism," in *Proceedings of the Advances in Bridge Aerodynamics*, Balkema, Rotterdam, The Netherlands, pp. 189–211, May 1998.

[20] J. A. Main and N. P. Jones, "Full scale measurements of stay cable vibration," in *Proceedings of the 10th International Conference on Wind Engineering*, pp. 963–970, Copenhagen, Denmark, June 1999.

[21] A. J. Persoon and K. Noorlander, "Full scale measurements on the Erasmus Bridge after rain/windinduced cable vibration," in *Proceedings of the 10th International Conference on Wind Engineering*, pp. 1019–1026, Copenhagen, Denmark, June 1999.

[22] S. Kumarasena, N. Jones, P. Irwin, and P. Taylor, *Wind-Induced Vibration of Stay Cables*, Wiley, Hoboken, NJ, USA, 2007.

[23] A. Acampora and C. T. Georgakis, "Recent monitoring of the Oresund Bridge: rain–wind induced cable vibrations," in *Proceedings of the 13th International Wind Engineering Conference*, p. 2011, Amsterdam, Netherland, July 2011.

[24] M. Gu and Q. Lu, "Theoretical analysis of wind- rain induced vibration of cables of cable- stayed bridges," *Wind Engineering and Industrial Aerodynamics*, vol. 89, pp. 125–128, 2001.

[25] O. Flamand, "Rain/wind-induced vibration of cables," in *Proceedings of the International Conference on Cable-Stayed and Suspension Bridges (AFPC)*, pp. 523–531, Deauville, France, October 1994.

[26] A. Bosdogianni and D. Olivari, "Wind- and rain-induced oscillations of cables of stayed bridges," *Journal of Wind Engineering and Industrial Aerodynamics*, vol. 64, no. 2-3, pp. 171–185, 1996.

[27] G. L. Larose and L. W. Smitt, "Rain/wind induced vibrations of parallel stay cables," in *Proceedings of the IABSE Conference, Cable-Stayed Bridges—Past, Present and Future*, Malmo, Sweden, June 1999.

[28] N. Coesentino, O. Flamand, and C. Ceccoli, "Rain–wind-induced vibration of inclined stay cables. Part I: experimental investigation and physical explanation," *Wind Engineering and Industrial Aerodynamics*, vol. 93, pp. 79–95, 2005.

[29] M. Gu and X. Du, "Experimental investigation of rain–wind-induced vibration of cables in 369 cable-stayed bridges and its mitigation," *Wind Engineering and Industrial Aerodynamics*, vol. 93, no. 79–95, 2005.

[30] H. Katsuchi, H. Yamada, I. Sakaki, and E. Okado, "Wind-tunnel investigation of the aerodynamic performance of surface-modification cables," *Engineering*, vol. 3, no. 6, pp. 817–822, 2017.

[31] Y. Ge, Y. Chang, L. Xu, and L. Zhao, "Experimental investigation on spatial attitudes, dynamic characteristics and environmental conditions of rain-wind-induced vibration of stay cables with high-precision raining simulator," *Journal of Fluids and Structures*, vol. 76, pp. 60–83, 2018.

[32] J. A. Main and N. P. Jones, "Evaluation of viscous dampers for stay-cable vibration mitigation," *Journal of Bridge Engineering*, vol. 6, no. 6, pp. 385–397, 2001.

[33] E. A. Johnson, G. A. Baker, B. F. Spencer, and Y. Fujino, "Semiactive damping of stay cables," *Journal of Engineering Mechanics*, vol. 133, no. 1, pp. 1–11, 2007.

[34] W. Wu and C. S. Cai, "Theoretical exploration of a taut cable and a TMD system," *Engineering Structures*, vol. 29, pp. 962–972, 2006.

[35] I. F. Lazar, S. A. Neild, and D. J. Wagg, "Vibration suppression of cables using tuned inerter dampers," *Engineering Structures*, vol. 122, pp. 62–71, 2016.

[36] S. Elias and V. Matsagar, "Research developments in vibration control of structures using passive tuned mass dampers," *Annual Reviews in Control*, vol. 44, pp. 129–156, 2017.

[37] C. H. Nguyen and J. H. G. Macdonald, "Galloping analysis of a stay cable with an attached viscous damper considering complex modes," *Journal of Engineering Mechanics*, vol. 144, no. 2, 2018.

[38] H. Katsuchi and H. Yamada, "Wind-tunnel study on dry-galloping of indented-surface stay cable," in *Proceedings of the 11th Americas conference on wind engineering*, pp. 22–26, Puerto Rico, USA, June 2009.

[39] H. D. Vo, H. Katsuchi, H. Yamada, and M. Nishio, "Experimental study on dry-state galloping with various wind relative angles and its countermeasures," *Journal of Structural Engineering*, vol. 60A, pp. 428–436, 2014.

[40] H. Jing, Y. Xia, H. Li, Y. Xu, and Y. Li, "Excitation mechanism of rain–wind induced cable vibration in a wind tunnel," *Journal of Fluids and Structures*, vol. 68, no. 32–47, 2017.

[41] D. Yeo and N. P. Jones, "Investigation on 3-D characteristics of flow around a yawed and inclined circular cylinder," *Journal of Wind Engineering and Industrial Aerodynamics*, vol. 96, no. 10-11, pp. 1947–1960, 2008.